

NMR Analyses of the Activation of the Arp2/3 Complex by Neuronal Wiskott–Aldrich Syndrome Protein[†]

Mara Kreishman-Deitrick,^{‡,§} Erin D. Goley,^{||} Lyle Burdine,[⊥] Carilee Denison,[⊥] Coumaran Egile,[#] Rong Li,[#] Nagarajan Murali,[△] Thomas J. Kodadek,[⊥] Matthew D. Welch,^{||} and Michael K. Rosen^{*,‡}

Department of Biochemistry and Center for Biomedical Inventions, University of Texas Southwestern Medical Center, Dallas, Texas 75390, Department of Molecular and Cell Biology, University of California, Berkeley, California 94720, Stowers Institute for Medical Research, 1000 East 50th Street, Kansas City, Missouri 64110, and Varian Instruments, Palo Alto, California 94304

Received June 4, 2005; Revised Manuscript Received September 28, 2005

ABSTRACT: The VCA domain of the neuronal Wiskott–Aldrich syndrome protein (N-WASP) is a potent activator of the Arp2/3 complex, a 240 kDa heteroheptameric actin-nucleating assembly. We used site-directed spin labeling of N-WASP peptides in conjunction with methyl-TROSY spectra of the intact, selectively labeled Arp2/3 complex to identify regions of the VCA that are proximal to the ARPC3 subunit of the assembly. We also cross-linked CA peptides to the Arp3, Arp2, ARPC1, and ARPC3 subunits. The combined data suggest that the extreme C-terminus of the A region and the C-terminus of the C region of N-WASP are proximal to ARPC3. These results have implications for the mechanism of Arp2/3 complex activation by VCA peptides. This study also demonstrates the utility of NMR spectroscopy for studying ligand binding events in large, asymmetric, macromolecular assemblies.

Many cellular processes depend on rapid, tightly regulated polymerization of new actin filaments, including motility, differentiation, changes in morphology, intercellular spread of bacterial and viral pathogens, and tumor metastasis. The second time scale actin dynamics seen in cells must be reconciled, however, with the fact that polymerization of isolated actin is preceded by an unfavorable nucleation event that creates a significant time lag in the generation of new filaments. In the creation of branched filament networks, the cell overcomes this barrier to polymerization through the use of an actin nucleation factor, the actin-related protein (Arp) 2/3 complex.

The Arp2/3 complex¹ is a constitutive 240 kDa assembly of seven polypeptides: actin-related proteins 2 and 3 and five novel proteins [referred to as Arp complex (ARPC) 1 through 5]. The purified Arp2/3 complex promotes nucleation poorly, but its activity can be significantly enhanced by the cooperative effects of preexisting filaments and nucleation promoting factors (NPFs), such as members of the Wiskott–Aldrich syndrome protein family (1). Arp2 and Arp3 are

highly homologous to actin, and a central tenet of current models for Arp2/3 complex function is that these subunits form a pseudo-actin dimer during nucleation (2). However, in the crystal structure of the inactive Arp2/3 complex, Arp2 and Arp3 are separated by a large cleft, displaced from their predicted positions in an actin filament (2–4). Thus, activation is believed to critically involve a conformational change in the Arp2/3 complex that reorganizes Arp2 and Arp3. This model is supported by observations that when CFP and YFP are attached to the ARPC3 and ARPC1 subunits of the Arp2/3 complex, respectively, fluorescence resonance energy transfer (FRET) between the fluorophores increases upon activation by WASP, suggesting a rearrangement that brings the subunits closer together (5). Additionally, electron microscopy analyses demonstrate that WASP can bias the conformational equilibrium of the Arp2/3 complex from an

¹ Abbreviations: 462*, 481*, and 506*, N-WASP CA peptides derivatized with a nitroxide spin label at residue position 462, 481, and 506, respectively; A region, acidic C-terminal region of the VCA; ARPC1, Arp complex protein 1; Arp2, actin-related protein 2; Arp3, actin-related protein 3; Arp2/3 complex, actin-related protein 2/actin-related protein 3 complex; Bee1, yeast WASP-like protein; C region, central hydrophobic region of the VCA; CA peptide, peptide containing C and A regions of the N-WASP VCA domain; CFP, cyan fluorescent protein; CRIPT, cross-relaxation-induced polarization transfer; DOPA, dihydroxyphenylalanine; DOPA(462)-CA peptide, N-WASP CA peptide with DOPA substituted at residue position 462; EDC, 1-ethyl-3-(3-dimethylaminopropyl)carbodiimide; FRET, fluorescence resonance energy transfer; GBD, GTPase binding domain; HMQC, heteronuclear multiple-quantum coherence HRP, horseradish peroxidase; HSQC, heteronuclear single-quantum coherence; N-WASP, neuronal Wiskott–Aldrich syndrome protein; NMR, nuclear magnetic resonance; NPF, nucleation promoting factor; SDSL, site-directed spin labeling; TROSY, transverse relaxation optimized spectroscopy; V region, verprolin-homology region of the VCA; VCA, C-terminal domain of WASP/Scar proteins containing a verprolin-homology region, a central hydrophobic region, and an acidic region; WASP, Wiskott–Aldrich syndrome protein; YFP, yellow fluorescent protein.

[†] Supported by grants from the NIH (P01GM066311 to M.K.R. and R.L. and GM59609 to M.D.W.) and the Welch Foundation (I1544 to M. K. R.). E.D.G. is supported by an NSF graduate research fellowship.

* To whom correspondence should be addressed. E-mail: mrosen@biochem.swmed.edu. Phone: 214-645-6361. Fax: 214-645-6353.

[‡] Department of Biochemistry, University of Texas Southwestern Medical Center.

[§] Current address: Division of Experimental Therapeutics, Walter Reed Army Institute of Research, 503 Robert Grant Ave., Silver Spring, MD 20910.

^{||} University of California, Berkeley.

[⊥] Center for Biomedical Inventions, University of Texas Southwestern Medical Center.

[#] Stowers Institute for Medical Research.

[△] Varian Instruments.

open state containing a large cleft [consistent with the bovine crystal structure (2)] toward a more compact conformation (6, 7). Both studies are consistent with an activation model in which Arp2 and Arp3 undergo a quaternary rearrangement that brings them into a filament-like conformation (Figure 1). Activation is also concomitant with hydrolysis of ATP by Arp2, a reaction stimulated by the actin monomer (8). It is not known if hydrolysis is coupled to NPF-mediated conformational changes or is an independent process. The mechanisms by which these different aspects of activation are coordinated by NPFs, filaments, and the actin monomer are not well understood.

Proteins in the Wiskott–Aldrich syndrome protein (WASP) family activate the Arp2/3 complex through a conserved C-terminal element termed the VCA domain. The VCA can be divided into three distinct functional segments: a *ver*-prolin-homology sequence, which binds actin monomers and may recruit them to the Arp2-Arp3 dimer (8), a hydrophobic central region required for Arp2/3 activation, and an acidic tail required for high-affinity binding of VCA to the Arp2/3 complex (9–11). In efforts to map activator contact sites on the Arp2/3 complex, VCA peptides have been chemically cross-linked to Arp3, Arp2, ARPC1, and ARPC3 using the zero-length cross-linking reagent 1-ethyl-3-(3-dimethylaminopropyl)carbodiimide (EDC) (12–14). C-Terminally truncated VCA peptides retain the ability to cross-link to Arp2 and ARPC1, but cross-linking to Arp3 is severely decreased, suggesting that Arp3 may contain the binding site for the acidic region (14, 15). However, recent direct binding data suggest that the VCA C-terminus may contact the ARPC1 subunit (16). The relative positions of the N-terminal V and C portions of VCA have not yet been examined experimentally. The position of the C region is particularly important because its contacts are necessary to drive an activation step during the nucleation process (9, 10).

Candidate VCA binding sites on the surface of the Arp2/3 complex were recently proposed on the basis of homology modeling of the assembly from seven species (17). A candidate binding site composed of three patches, one each on Arp3, Arp2, and ARPC3, was identified that would be compatible with the lengths and charge distributions of the C and A regions. Interestingly, the patches on Arp2 and ARPC3 are displaced from one another in the inactive complex, but a conformational change creating an Arp2-Arp3 pseudo-actin dimer would make them adjacent.

Here we present NMR investigations of the intact, selectively labeled Arp2/3 complex and complementary cross-linking studies to better understand the interactions of the assembly with VCA peptides. The data suggest that CA binds to Arp3, Arp2, ARPC1, and ARPC3, with the C-terminus of the C region and the C-terminus of the A region proximal to ARPC3. The N-terminus of the C region appears to be distal to ARPC3 and may interact with an actin monomer and/or other cross-linking subunits of the Arp2/3 complex. This work also demonstrates the applicability of methyl-TROSY NMR techniques to understanding the structure, ligand interactions, and dynamics of very large macromolecular systems.

MATERIALS AND METHODS

Protein Expression and Purification. All chromatography resins were obtained from Amersham Biosciences unless

otherwise indicated. The bovine Arp2/3 complex, human neuronal WASP (N-WASP) CA peptides (residues 458–505), the N-WASP GTPase binding domain (GBD, residues 192–275), U-²H/¹²C/¹⁵N/¹H,¹³C(methyl)-ARPC3, and the selectively labeled yeast Arp2/3 complex were all purified as described previously (18–20).

The recombinant human Arp2/3 complex lacking ARPC3 was expressed in insect cells essentially as described previously (21) except that a Flag-His₆-tagged version of ARPC1 was employed to facilitate purification. Briefly, HighFive cells (Invitrogen) were infected with four recombinant baculoviruses expressing one or two subunits each (Arp3, Arp2/ARPC5, ARPC2/ARPC4, ARPC1-Flag-His₆) at a multiplicity of infection of 2 each for 72 h with shaking at 27 °C. Infected cells were harvested by centrifugation, washed once in phosphate-buffered saline (10 mM sodium phosphate, pH 7.4, 150 mM NaCl), frozen in liquid nitrogen, and stored at –80 °C.

Frozen cells from 2 to 8 L of culture were resuspended in 1 volume of lysis buffer (50 mM Tris, pH 8.0, 300 mM NaCl, 10 mM imidazole, 1 mM MgCl₂, 1 mM EGTA, 10% glycerol, 0.1% Brij-58, 1 mM PMSF, 1 mg/mL each benzamidine, leupeptin, antipain, and pepstatin A) and lysed by thawing in a room temperature water bath. The lysate was cleared by centrifugation at 240000g for 15 min. The cleared lysate was applied to 9 mL of Ni-NTA agarose (Qiagen) equilibrated in 5–10 volumes of lysis buffer and incubated with gentle shaking in batch for 30 min at 4 °C. The flow-through was collected by gravity flow, and the resin was washed with 20 column volumes of wash buffer (50 mM Tris, pH 8.0, 300 mM NaCl, 20 mM imidazole, 1 mM MgCl₂, 1 mM EGTA, 10% glycerol, 0.1% Brij-58). The mutant complex was eluted from the resin with 4 times 2 column volumes of elution buffer (50 mM Tris, pH 8.0, 300 mM NaCl, 300 mM imidazole, 1 mM MgCl₂, 1 mM EGTA, 10% glycerol, 0.1% Brij-58). Eluates containing the mutant complex were pooled (Figure 2a), and labeled ARPC3 was added in approximately 5-fold molar excess, followed by incubation at 4 °C for 1 h. The reconstituted complex was incubated 4–6 h at room temperature with 2000–30000 units of Tev protease (Invitrogen) to cleave the His₆ tag. The solution could not be concentrated prior to Tev cleavage due to low solubility of the tagged partially purified complex. The completed cleavage reaction was diluted 12-fold in Mono-S buffer A (10 mM PIPES, pH 6.8, 1 mM EGTA, 1 mM MgCl₂, 10% glycerol; buffer B = buffer A with 1 M NaCl), and the complex was purified by cation-exchange (Mono-S) and gel filtration (Superdex 200, buffer = 25 mM phosphate, pH 7.0, 50 mM NaCl, 1 mM EGTA, 1 mM MgCl₂, 1 mM DTT, 10% glycerol) chromatographies (panels b and c of Figure 2, respectively). The Mono-S step was particularly important because this column serves to separate reconstituted complex from other, nonstoichiometric sub-complexes. Subunit stoichiometry in the final, reconstituted assembly was verified by SDS–PAGE (Figure 2c). The complex was then exchanged into NMR buffer (Superdex 200 buffer with 100% D₂O) containing 10% glycerol-*d*₈, 0.5 mM ATP, and protease inhibitors (1 mM benzamidine, 1 μg/mL each leupeptin and antipain) by multiple cycles of concentration and dilution using a Centriplus-30 concentrator (Amicon). Glycerol (10%) was added to the samples to increase the solubility of the reconstituted assembly. The complex for site-directed spin-labeling (SDSL) studies was

purified using gel filtration buffer without DTT. Under these conditions, concentrated, labeled complex is stable at room temperature for approximately 3 days with no signs of degradation and minimal precipitation. Spin-labeled CA peptides were added from concentrated stock solutions (≥ 1 mM) to the buffer-exchanged, concentrated complex at a 1:1 molar ratio.

Cysteine was introduced into CA peptides for SDSL experiments using the QuikChange site-directed mutagenesis kit (Stratagene). For spin labeling, each peptide was incubated in 25 mM sodium phosphate, pH 7.0, and 100 mM NaCl with a 20-fold molar excess of 3-maleimido-PROXYL (Aldrich, dissolved at 25 mg/mL in acetone) at 4 °C for 12–16 h. Labeled peptides were separated from excess PROXYL reagent by gel filtration chromatography. Labels were introduced at residue positions 462, 481, and 506, and the corresponding labeled peptides will be referred to as 462*, 481*, and 506*, respectively.

NMR Spectroscopy. The Arp2/3 complex concentration in NMR samples ranged from 28 to 56 μ M, as listed in the legend to Figure 3. $^1\text{H}/^{13}\text{C}$ heteronuclear multiple-quantum coherence (HMQC) spectra of the Arp2/3 complex were acquired on a Varian Inova 600 MHz spectrometer equipped with a cold probe, with sweep widths of 15 ppm (^1H) and 31 ppm (^{13}C), t_2 and t_1 acquisition times of 64 and 28 ms, respectively, a transfer delay of 1.7 ms, and a recycle delay of 1.1 s (delays optimized empirically). The total acquisition time was 56 h for all samples except the complex of reduced 506* (see previous Materials and Methods section for nomenclature of spin-labeled peptides), where the acquisition time was 88 h. All CA-bound spectra were acquired on the same 600 MHz spectrometer using the same probe, with the exception of the reduced 506* spectrum. Spectra were processed in NMRPipe using a cosine-squared window function. Peak picking and signal-to-noise (S/N) analyses were performed using NMRDraw (22). S/N ratios were calculated for 22 of the 38 peaks in each spectrum and normalized for the different sample concentrations. For each peak, the ratio of normalized S/N in the spin-labeled and unlabeled reference spectrum was calculated. Error bars were calculated in NMRDraw from standard errors in the fit for each intensity measurement based on the noise in each spectrum (22). These errors were propagated using the standard equation for error propagation in a ratio. Peaks in the reference spectrum with S/N less than 15 were excluded from quantitation.

Photoinduced Cross-Linking. The CA-Arp2/3 complex and GBD competition cross-linking reactions (20 μ L) were performed as described (23) in KMEI buffer (10 mM imidazole, pH 7.0, 50 mM KCl, 1 mM EGTA, 1 mM MgCl_2). Protein concentrations are given in the legend of Figure 4. Cross-linked products were separated on SDS-PAGE gels and visualized by Western blotting with antibodies against human Arp3, Arp2, ARPC1, ARPC2, and ARPC3. Antibodies against Arp3 and ARPC2 were purchased from Upstate. Antibodies against Arp2 and ARPC3 were purchased from Santa Cruz Biotechnology and BD Biosciences, respectively.

DOPA-Mediated Cross-Linking of the Synthetic CA Peptide to the Arp 2/3 Complex. The biotinylated dihydroxyphenylalanine (DOPA) containing peptide was obtained from Anaspec (San Jose, CA). The sequence was PXPTS-GIVGALMEVMQKRSKAIHSSDEDEDEDEDEFEDDDE-

WEDGGZ, where X = 3,4-dihydroxyphenylalanine and Z = biotinylated glutamic acid. An endogenous alanine was replaced with the artificial DOPA residue in this peptide. Cross-linking reactions were carried out in 40 μ L of KMEI buffer containing 1 mM DTT. The purified Arp2/3 complex was equilibrated with the peptide for 10 min at room temperature, and then NaIO_4 was added to a final concentration of 1 mM to trigger the cross-linking reaction. After 30 s the reaction was stopped with the addition of 6 \times SDS protein loading buffer (with 1% SDS) containing 100 mM β -mercaptoethanol. The samples were then boiled and loaded onto a 4–20% SDS-PAGE gradient gel. The gel was either stained or transferred to a PVDF membrane for Western blotting according to standard procedures. NeutrAvidin-HRP was diluted 1:2500 from a stock solution of 1 mg/mL to probe the Western blot for biotinylated products.

RESULTS

Analysis of CA Interaction with ARPC3 by NMR Using SDSL. To examine interactions of the Arp2/3 complex with VCA peptides, our plan was to label a single subunit of the assembly with NMR-active nuclei, leaving the remaining subunits unlabeled. The VCA binding site could then be mapped by observing perturbations in the labeled subunit induced by WASP peptides. We and others have found that, for model systems with very long correlation times (> 100 ns), $^1\text{H}/^{13}\text{C}$ heteronuclear single-quantum coherence (HSQC) spectra of protonated methyl groups in a fully deuterated background provide much higher sensitivity than do spectra such as $^1\text{H}/^{15}\text{N}$ -CRIPT-TROSY designed to observe backbone amides (18, 24). Moreover, Tugarinov et al. have demonstrated that, for isolated methyl groups, a TROSY effect resulting from cancellation of intramethyl dipolar relaxation interactions gives even higher sensitivity in $^1\text{H}/^{13}\text{C}$ HMQC spectra (25). Thus, our efforts here focused on using $^1\text{H}/^{13}\text{C}$ HMQC analyses of methyl groups in the selectively labeled Arp2/3 complex.

We chose to label the ARPC3 subunit for observation because cross-linking (13), deletion (18), and yeast two-hybrid (11) analyses had indicated that this subunit is involved, either directly or indirectly, in activation of the Arp2/3 complex by VCA. Moreover, since ARPC3 only contacts a single additional subunit in the Arp2/3 complex (Arp3, Figure 1), recombinant, bacterially expressed ARPC3 can be incorporated on a milligram scale into mutant yeast and human complexes lacking this subunit to reconstitute their activities (18). We previously described the purification and preliminary NMR analysis of the reconstituted yeast assembly (18). This system, while useful for initial experiments, has a number of problems that make it less suitable for the quantitative, mechanistic studies described here. First, the mutant yeast assembly was reconstituted with human ARPC3, resulting in a complex with components from two species. Second, this hybrid assembly was unstable in solution and prone to rapid aggregation and precipitation over 12–24 h at the concentrations used for NMR. Finally, likely because of these problems, the reconstituted yeast assembly gave spectra of insufficient quality for quantitative analysis. Here we describe the reconstitution and purification of the recombinant human Arp2/3 complex labeled at ARPC3 (see Materials and Methods for details), which overcomes all of these issues. As was the case for the yeast assembly, exogenous ARPC3 was able to incorporate into a hexameric

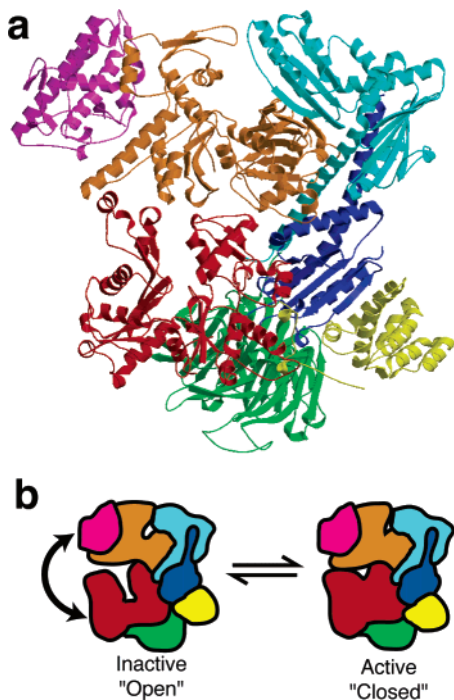


FIGURE 1: (a) Ribbon diagram of the crystal structure of the inactive bovine Arp2/3 complex (2). (b) Schematic representation of the hypothetical conformational equilibrium describing activation of the Arp2/3 complex. The assembly exists in two conformations: an inactive, open structure and an active, closed structure [both described in Robinson et al. (2)]. The closure of the cleft between the Arp proteins is shown by a curved arrow. Subunit colors are as follows: Arp3, orange; Arp2, red; ARPC1, green; ARPC2, cyan; ARPC3, magenta; ARPC4, blue; ARPC5, yellow. The ribbon diagram was created with Molscript (39).

mutant complex lacking that subunit. The hexameric assembly, which was His₆-tagged at the ARPC1 subunit, was expressed in insect cells and purified from cell lysate by Ni²⁺-affinity chromatography (Figure 2a). Addition of excess bacterially expressed and separately purified human ARPC3 gave high yields of the reconstituted heptameric Arp2/3 complex. ARPC3 did not incorporate into 100% of the available mutant complex, presumably because the hexameric assembly is destabilized and a population of that complex is not competent to bind ARPC3. Partial subcomplexes and excess ARPC3 could be purified away from the fully reconstituted assembly by cation-exchange chromatography (Figure 2b). The integrity of the final labeled complex was verified by its elution as a single peak from cation-exchange and gel filtration columns (Figure 2c). Retention times on gel filtration columns were characteristic of the intact human Arp2/3 complex expressed in insect cells (5). The stoichiometry of the subunits was verified by SDS-PAGE (Figure 2c). The assembly reconstituted with U-²H/¹²C/¹⁵N/¹H,¹³C-(methyl)-ARPC3 had high activity when stimulated with the WASP VCA (Figure 2d). However, activity was somewhat lower than the Arp2/3 complex purified from bovine thymus. Previous reconstitution experiments showed that recombinant unlabeled ARPC3 could restore full activity to a hexameric assembly lacking this subunit (21). Thus, while the reasons for the lower activity of our reconstituted material here are uncertain, they probably include the effects of deuteration of ARPC3.

As shown in Figure 3a, ¹H/¹³C HMQC spectra of the recombinant human Arp2/3 complex reconstituted with

deuterated, ¹H/¹³C-methyl-labeled ARPC3 are of high quality. As predicted, the ¹H/¹³C HMQC spectrum of the 240 kDa assembly is of considerably higher quality than its HSQC counterpart [compare with Figure S1 (Supporting Information), an HSQC spectrum]. In a typical spectrum of the 56 μM Arp2/3 complex bound to an N-WASP CA peptide recorded in 56 h, we can observe 38 of 51 expected methyl signals, with signal-to-noise (S/N) ratios ranging from 9 to 120 (Figure 3b). The crystal structure of the Arp2/3 complex does not show any evidence for disordered or highly mobile elements in ARPC3, so we expect that all peaks in our spectra likely represent folded, ordered portions of the subunit. It is therefore remarkable that some resonances do show very high S/N values, and this speaks to the robustness of the methyl HMQC method for detection of signals in large, asymmetric systems. As was the case with HSQC spectra, Ile signals are more intense than those from Leu and Val side chains due to intraregion ¹H-¹H dipolar interactions between the diastereotopic methyl groups within the latter residue types, which degrade the methyl-TROSY effect (25). These data are of sufficient quality for use in understanding WASP interactions with the Arp2/3 complex.

While the full VCA domain (human N-WASP residues 383–505) is required for activation of the Arp2/3 complex, the V region is believed to function primarily in recruitment of monomeric actin (1), while the CA probably drives conformational changes in the assembly (9, 10) and mediates binding affinity [e.g., CA and VCA have identical affinities for the Arp2/3 complex (10)]. Thus, to simplify our analyses, we used CA peptides in all of our NMR studies. Surprisingly, given previous biochemical and structural analyses (see introduction), only minor spectral perturbations are seen on addition of an unlabeled CA peptide to the free assembly (compare panels a and b of Figure 3). This suggests that there are only minimal or no direct contacts between ARPC3 and CA. To extend the distance through which CA could influence ARPC3 magnetization, we examined use of site-directed spin labeling (SDSL).

SDSL involves the observation of distance-dependent broadening of NMR resonances in samples containing specifically bound paramagnetic species, namely, metals or nitroxide spin labels. A key advantage of SDSL is that because the magnetic moment of the unpaired electron is several hundred times larger than those of NMR-observable nuclei, spin-label-induced broadening is detectable at long distances out to about 25 Å (26). This becomes important in terms of sensitivity in detecting ligand binding to asymmetric protein systems such as the Arp2/3 complex, where a single labeled subunit is used as a reporter for possible binding to multiple, distal subunits. On the basis of cross-linking data, the CA domains of the WASP/Scar proteins may span up to 80–100 Å or more when bound to the Arp2/3 complex, including the four-turn C region helix, up to 15 linker residues, and the C-terminal six residues of the A segment (13, 14, 17). By engineering spin labels at different points along the length of the CA peptide, we anticipated that it would be possible to detect differential broadening of ARPC3 resonances and thereby determine which regions of the CA bind on or within 25 Å of ARPC3.

We constructed a series of N-WASP CA peptides each containing a single amino acid conversion to cysteine, where we attached a maleimide-derivatized nitroxide spin label. The

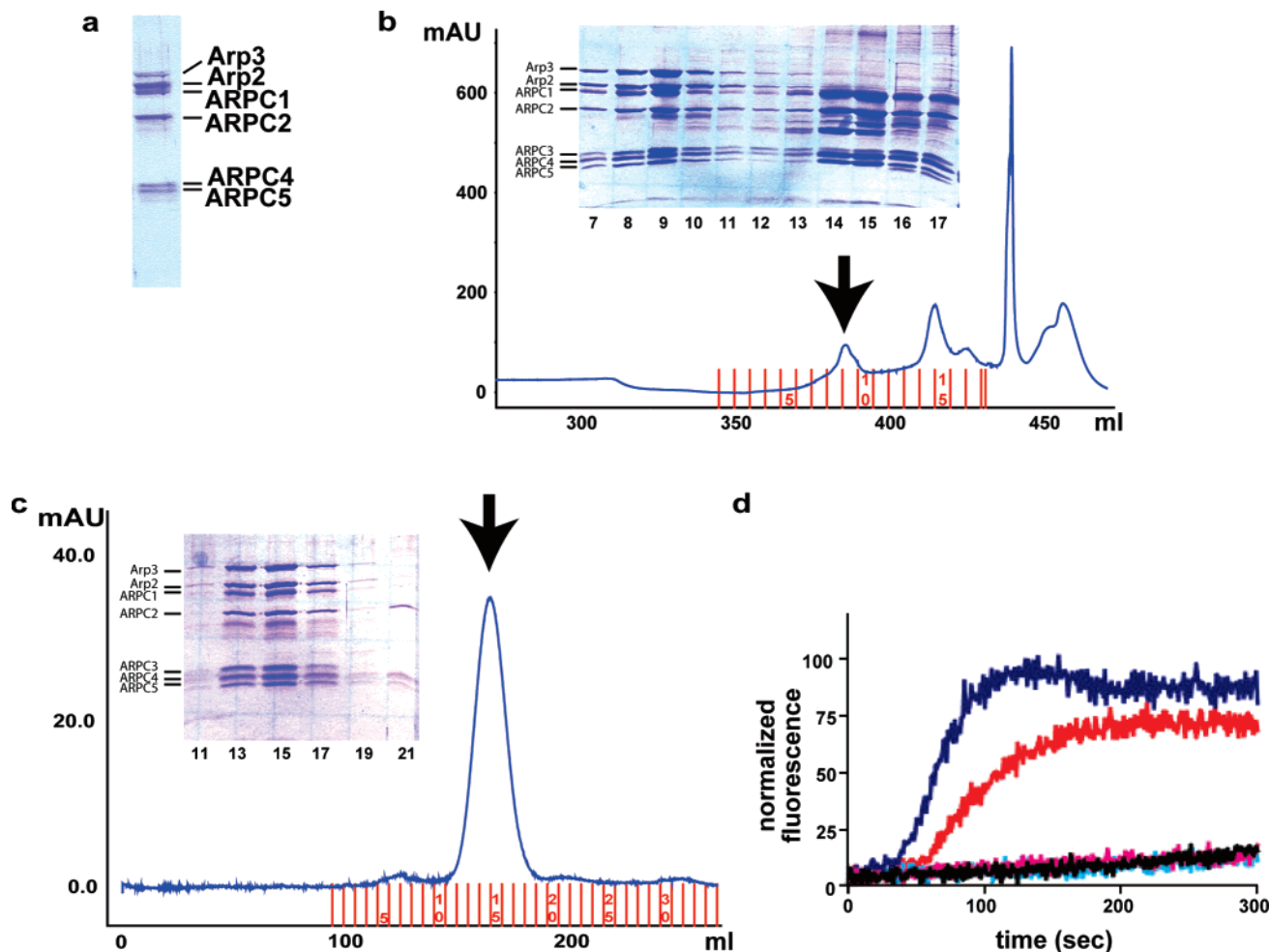


FIGURE 2: Reconstitution of the ARPC3-labeled Arp2/3 complex. (a) Coomassie blue stained SDS-PAGE gel of the His₆-tagged hexameric Arp2/3 complex, lacking ARPC3, eluted from Ni²⁺-affinity resin. (b) Cation-exchange chromatography of the reconstituted Arp2/3 complex. Absorbance at 280 nm is shown. Column fractions are indicated in red. The peak containing the heptameric Arp2/3 complex is indicated by the arrow. The inset shows the Coomassie blue stained SDS-PAGE gel of column fractions. (c) Gel filtration chromatogram of the reconstituted Arp2/3 complex. Labeling and inset are as in panel b. (d) Activity of the reconstituted Arp2/3 complex. Actin (4 μ M, 5.5% pyrene-labeled) was polymerized alone (black) or in the presence of 10 nM bovine Arp2/3 complex (magenta), 10 nM bovine Arp2/3 complex + 500 nM WASP VCA (blue), 10 nM reconstituted Arp2/3 complex (cyan), or 10 nM reconstituted Arp2/3 complex + 500 nM WASP VCA (red). Increase in fluorescence indicates incorporation of the actin monomer into filaments.

cysteine mutations are located at the N-terminus of the CA (A462C), at the C-terminus of the C region (A481C), and at the extreme C-terminus of the CA (C506, Figure 3a). The spin-labeled peptides will be referred to as 462*, 481*, and 506*, respectively, throughout the text. The locations of the three spin labels were chosen on the basis of previous NMR analyses of the VCA and its interactions with the Arp2/3 complex (9). Positions 481 and 506 were chosen on the basis of the finding that both of these residues are in regions of the peptide believed to interact directly with the Arp2/3 complex and, therefore, to be conformationally rigid. Other regions of the peptide, including the variable-length N-terminal portion of the A region, appear to be more mobile in the complex and may not make specific contacts to the Arp2/3 complex. Placement of spin labels in these regions would have left them mobile and more likely to cause nonspecific broadening effects. The spin label in the C region, 481*, was placed outside the probable binding face of the proposed amphipathic C region helix to avoid interfering with Arp2/3 complex binding (9). Analogous spin-labeled VCA peptides showed activities comparable to wild-type VCA in a pyrene-actin polymerization assay (not

shown), indicating that the labels do not perturb functionally important contacts of the CA peptides.

¹H/¹³C HMQC spectra of the ARPC3-labeled Arp2/3 complex bound to each of the three spin-labeled peptides are shown in Figure 3. Spin-label-induced broadening could be quantitated for 22 peaks in these spectra (panels g–i; see Materials and Methods for details). To ensure that the observed effects are specifically induced by the spin labels, an additional spectrum was acquired of the Arp2/3 complex bound to 506* and reduced by 1 mM sodium dithionite. One of the peaks whose intensity is recovered upon reduction is shown in the inset in Figure 3f, and a bar graph showing recovered intensity ratios for the rest of the spectrum is shown in Figure 3i. Reduction of the spin label clearly restores significant intensity in all of the methyl signals in ARPC3. A similar effect is seen on addition of sodium dithionite to the selectively labeled yeast Arp2/3 complex bound to 481* (data not shown). These data indicate that the lowered peak intensities observed in the presence of 481* and 506* are the direct result of the presence of a radical at those positions and that the nitroxide-induced line broadening will be useful in determining the orientation of the CA

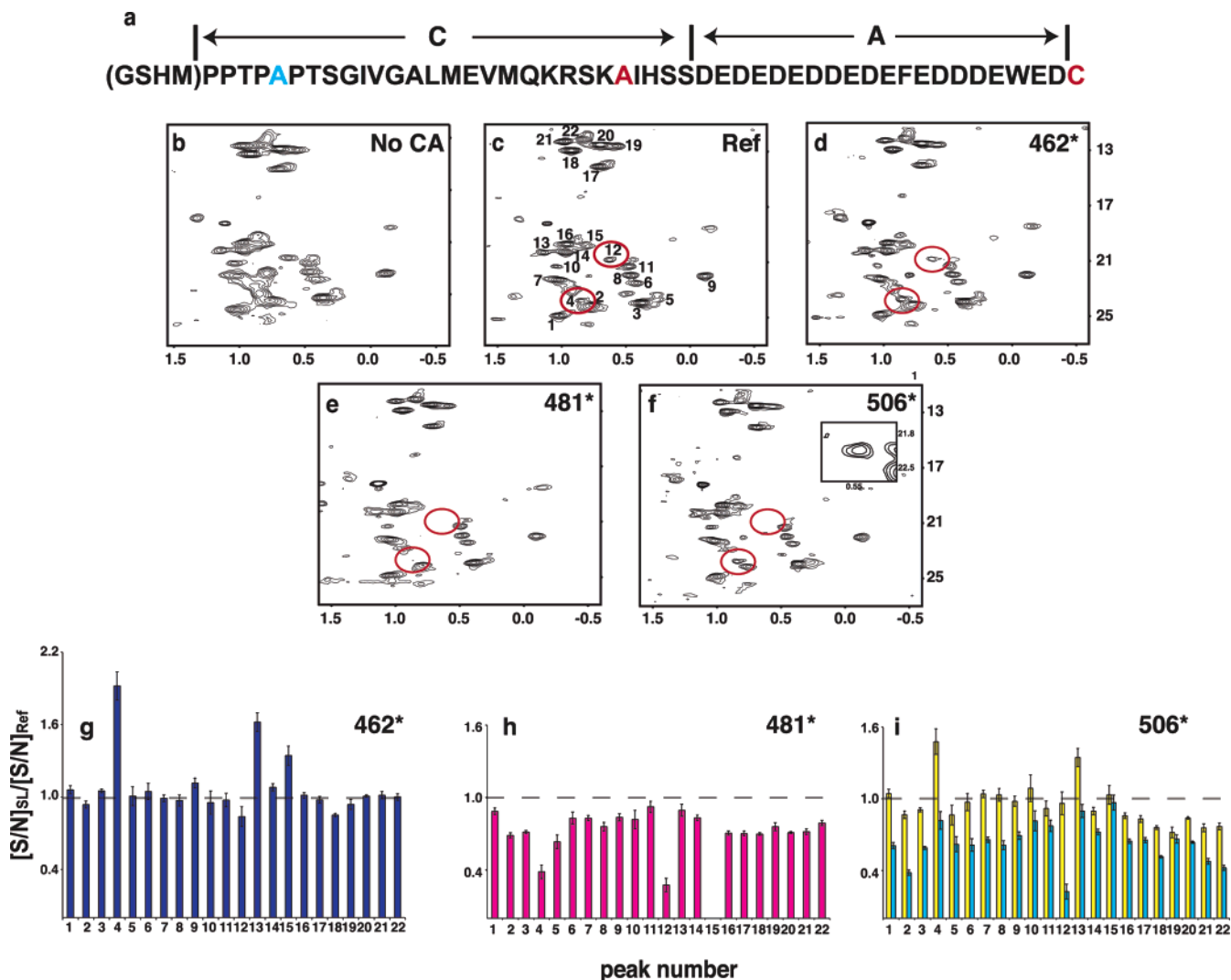


FIGURE 3: Analysis of CA interaction with ARPC3 by NMR using SDSL. (a) Sequence and region boundaries of the N-WASP CA peptide used for SDSL. Residue 462 (cyan) was used for both SDSL and DOPA labeling, and residue 481 and a cysteine introduced at position 506 (red) were used for SDSL. The four residues appended at the N-terminus of the peptide result from bacterial expression and subsequent purification and are shown in parentheses. (b) ¹H/¹³C HMQC spectrum of the recombinant human Arp2/3 complex labeled at ARPC3. (c–f) ¹H/¹³C HMQC spectra of the labeled recombinant human Arp2/3 complex in the presence of a 1:1 molar ratio of unlabeled CA (c) or each of the spin-labeled CA peptides indicated (d–f). Peak numbers are shown in (c). The two peaks showing the most dramatic, differential broadening are circled in red. The Arp2/3 complex concentrations are as follows: (c) 56 μM; (d) 40 μM; (e) 52 μM; and (f) 46 μM. The acquisition time was 56 h in all cases. Inset (f): peak number 12 in a ¹H/¹³C HMQC spectrum of the Arp2/3 complex bound to 506*, reduced with 1 mM sodium dithionite. (g–i) S/N ratio comparisons for the Arp2/3 complex SDSL spectra shown in (d–f). The ratio compares S/N in SDSL spectra to that in the reference spectrum: A462C-SL, blue bars; A481C-SL, magenta bars; C506-SL, cyan bars; C506-SL reduced (28 μM protein, 88 h acquisition time), yellow bars. A dotted line has been added at S/N = 1.0 on all bar graphs for visual comparison.

peptide with respect to ARPC3. While spin-label effects due to nonspecific electrostatic interactions of the highly charged A region with charged patches on the complex remain a possibility, the 1:1 stoichiometry of CA to the Arp2/3 complex in all of the NMR samples should minimize such effects.

Differential broadening effects are seen with each of the three peptides. Peptide 462* causes no appreciable decrease in the ARPC3 peak intensities, indicating that this position is distal to the labeled subunit. In contrast, both 481* and 506* induce significant broadening in a few ARPC3 methyl signals, suggesting that these two positions in the CA are proximal to ARPC3. These global aspects of the data suggest that the N-terminus of the C region helix is far from ARPC3, while the C-terminus of the helix and the extreme C-terminus

of the A region are located within approximately 25 Å of this subunit.

Although 481* and 506* both affect ARPC3 resonances, their effects are not identical. Analysis of relative peak intensities within each spectrum reveals that while both cause peak 12 to broaden almost to noise level, 506* also selectively broadens peak 2 (Figure 3g–i). Significant broadening is also observed for two to three other peaks for each label. However, the magnitude of broadening could not be accurately quantified due to weak intensity and/or overlap, and these peaks were not included in our analyses. Similarly, we also observe a more global reduction in peak intensities to 0.8 or less of the reference values in both 481* and 506*. This may reflect weak interactions of the mobile spin label with a large number of methyl signals in ARPC3 or weak

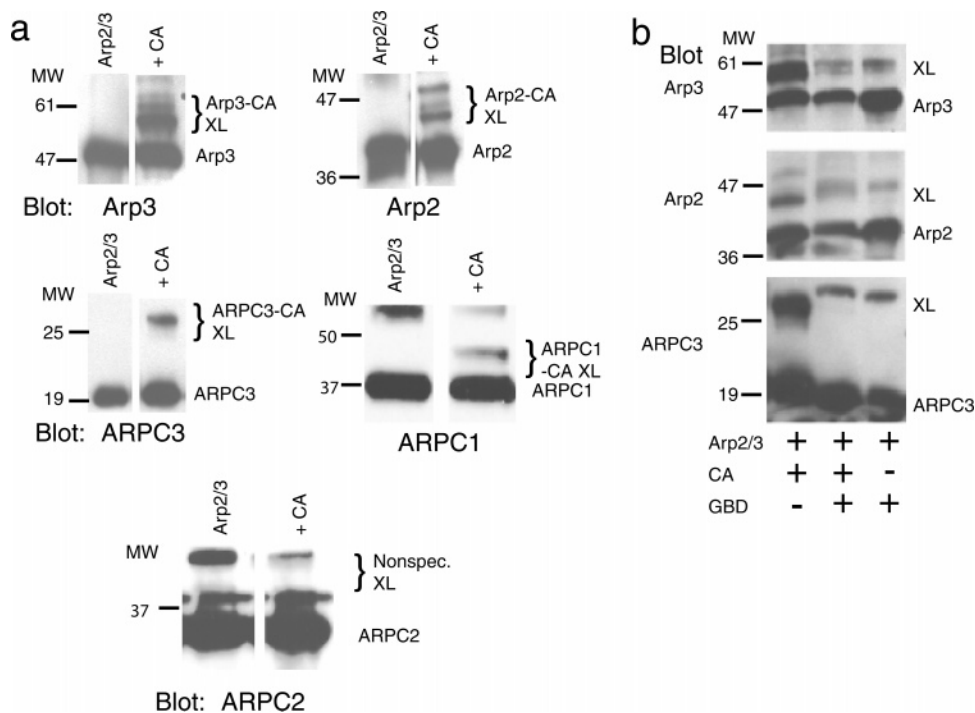


FIGURE 4: Cross-linking of CA peptides to Arp3, Arp2, and ARPC3. (a) Photoinduced cross-linking of wild-type N-WASP CA to the bovine Arp2/3 complex. Reactions contained 1 μ M Arp2/3 complex and 2 μ M peptide. Cross-linked products were separated on SDS-PAGE gels and detected by Western blotting for the subunits indicated. (b) Competition of Arp2/3-CA cross-linking with N-WASP GBD. Proteins were added to each photo-cross-linking reaction at the following concentrations: Arp2/3 complex, 1 μ M; CA, 5 μ M; GBD, 10 μ M. Products were separated and detected as in (a).

nonspecific binding of the CA peptide to additional sites on or near ARPC3. These more generalized, lower magnitude effects may also be due to sample-to-sample variation. As each of these spectra was recorded on a newly purified protein sample (as necessitated by the inability to store the purified complex for long periods as well as practical aspects of the purification procedure and the cost of insect cell culture and preparation of labeled material; see Materials and Methods), some sample-to-sample variability in intensities is to be expected, even after careful normalization for concentration and data acquisition parameters. The necessity of using a new sample for each spectrum emphasizes the inherent difficulties in studying complicated, reconstituted protein assemblies by NMR. Such protein systems are likely to suffer from suboptimal sample stability and solubility similar to what we have observed with the Arp2/3 complex. This limitation in sample number becomes an issue when looking at peaks where the ratio of spin label versus reference intensities is greater than 1 (see bar graphs, Figure 3). We assume that these anomalous values are due to sample-to-sample variations and have excluded these peaks from our analyses. The peaks on which we base our conclusions do show good reproducibility across different NMR samples.

In a previous study examining the utility of spin-label-induced relaxation in protein global fold determination by NMR, signals with measurable intensity ratios below 0.85 (with respect to a reduced control spectrum) were classified as within 14–23 Å of the label (26). By this same logic, the SDSL data for the three CA peptides suggest that CA binds to Arp2/3 in such a way that spin labels at positions 481 and 506, which flank the A region, are each within about 14–23 Å of at least one methyl-containing residue (and both proximal to the residue corresponding to peak 12). The spin

label at position 462, which is at the N-terminus of the C region helix, does not decrease the intensities of the ARPC3 methyl signals and must therefore be located farther away.

Cross-Linking of CA Peptides to Arp3, Arp2, ARPC1, and ARPC3. Chemical cross-linking has been successfully used to detect interactions of full-length VCA peptides with four Arp2/3 subunits (Arp3, Arp2, ARPC1, and ARPC3) (12–14). However, specific sites of cross-linking of each of the three functional regions of VCA have not been identified. Furthermore, the SDSL NMR data only tell us that two regions of the CA are close in space to ARPC3, not their actual binding sites. Therefore, we set out to delineate the subset of Arp2/3 complex subunits that interact physically with the CA peptide.

We used a cross-linking method based on light-activated metal complexes to probe the interaction of wild-type N-WASP CA with five subunits of the Arp2/3 complex: Arp3, Arp2, ARPC1, ARPC2, and ARPC3. This method uses a photoactivated ruthenium(II) complex to oxidatively cross-link associated proteins via aromatic and other nucleophilic side chains (27, 28). Using this technique, the CA peptide clearly cross-links to Arp3, Arp2, ARPC1, and ARPC3. The peptide does not appear to cross-link to ARPC2, although it is possible that CA-cross-linked products are obscured by two nonspecific slower migrating bands observed for this subunit even in the absence of CA (Figure 4a). The peptide induces multiple electrophoretically retarded bands for several of the subunits. While the reason for multiple bands is not certain, they may result from CA cross-linking to itself in addition to the Arp2/3 complex and also to the different electrophoretic mobility of products cross-linked to different residues on each subunit. Notably, for all four cross-linking subunits, CA-induced cross-linking induces electrophoretic

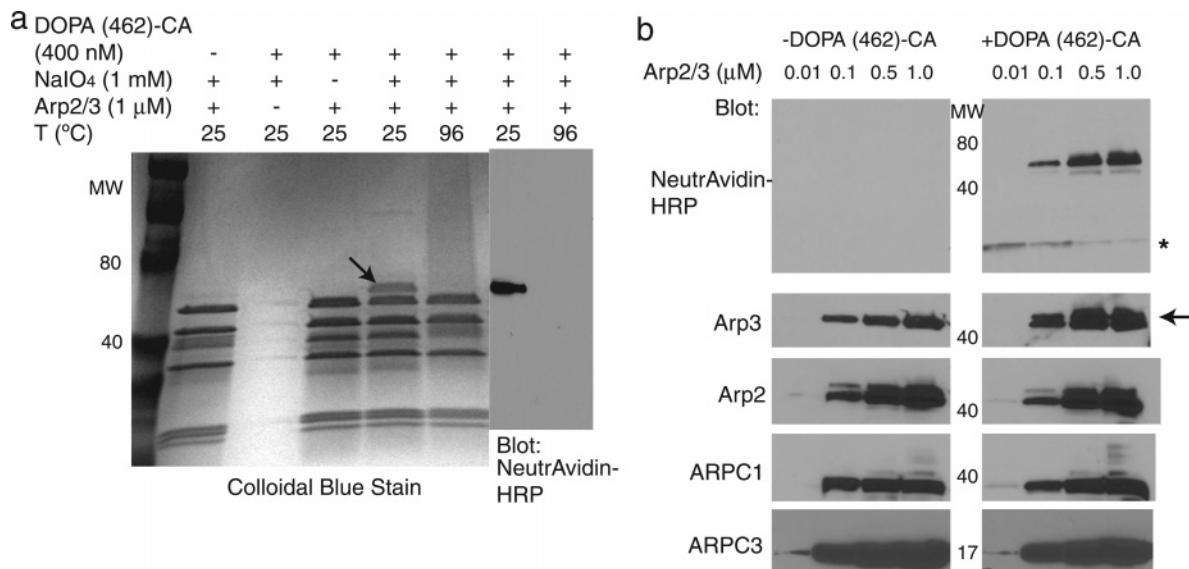


FIGURE 5: Cross-linking of the DOPA(462)-CA peptide to Arp3. (a) Periodate-mediated cross-linking of the DOPA(462)-CA peptide to the bovine Arp2/3 complex. Cross-linking reactions were separated on SDS-PAGE gels and either stained with Colloidal Blue (lanes 1–5) or transferred to a PVDF membrane and probed for biotinylated products (lanes 6 and 7). The arrow denotes the cross-linked product. (b) Periodate-mediated cross-linking of the DOPA(462)-CA peptide to the bovine Arp 2/3 complex. The DOPA(462)-CA peptide was present at 20 nM and incubated with 10 nM, 100 nM, 500 nM, and 1 μM of the Arp 2/3 complex. Cross-linked products were separated on SDS-PAGE gels and detected by Western blotting for the subunits as indicated. The star denotes free peptide. The arrow indicates product cross-linked to Arp3.

mobility shifts of roughly 6–12 kDa, consistent with direct cross-linking to CA and not to other Arp2/3 complex subunits, the smallest of which is 16 kDa.

To establish that the cross-linked products seen in Figure 4 are specifically induced by the CA peptide, competition experiments were performed using the N-WASP GTPase binding domain (GBD). The GBD of N-WASP has been shown to bind N-WASP VCA with $K_D = 2.8 \mu\text{M}$ and to inhibit the ability of N-WASP VCA to stimulate the activity of Arp2/3 complex, presumably by preventing interaction of the C region with the assembly (20, 29, 30). The intensity of the CA-cross-linked bands is efficiently lowered by 10 μM GBD (Figure 4b), indicating that the cross-linked products are indeed specifically induced by CA. Some nonspecific cross-linking of the GBD to the Arp2/3 complex is seen in this experiment, but the GBD cross-linked products are of a different electrophoretic mobility and significantly lower intensity than the CA cross-linked bands (compare Figure 4b, lanes 1 and 3). This indicates that the high-intensity, CA cross-linked band is efficiently replaced in each case by the nonspecific, low-intensity, GBD cross-linked band. Together, these data confirm that cross-linked products seen in previous VCA-Arp2/3 complex cross-linking studies are in fact due to direct interaction of Arp3, Arp2, ARPC1, and ARPC3 with CA.

Given that spin-label insertion at position 462 of the CA peptide does not decrease the intensities of the ARPC3 methyl signals, we sought to identify the Arp2/3 subunit that directly interacts with the N-terminus of the CA peptide. To accomplish this goal, we inserted the site-specific chemical cross-linker 3,4-dihydroxyphenylalanine (DOPA) into position 462 of a biotinylated CA peptide [to give DOPA(462)-CA peptide]. Periodate-mediated activation of DOPA results in the formation of an *o*-quinone capable of forming adducts with cysteine, histidine, and lysine. Importantly, cross-linking of activated DOPA-containing peptides to closely associated proteins occurs in high yield with little or no cross-linking

to nonassociated proteins (31, 32). In Figure 5a the DOPA(462)-CA peptide was added to a final concentration of 400 nM in a solution containing 1 μM Arp2/3 complex. After equilibrating the solution for 10 min, sodium periodate was added to a final concentration of 1 mM, and cross-linking was allowed to proceed for 30 s before the reaction was quenched. A strong cross-linked product was detected in the presence of periodate. This migrated slightly higher than Arp3 on an SDS-PAGE gel (Figure 5a, lane 4). The product was not produced under denaturing conditions at 96 °C (lane 5), in the absence of periodate (lane 3), in the absence of Arp2/3 (lane 2), or in the absence of the DOPA(462)-CA peptide. Western blotting with NeutrAvidin-horseradish peroxidase (HRP) revealed that the cross-linked product was biotinylated (lane 6) while mass spectrometric analysis of the cross-linked product indicated that the band of interest contained Arp3 (data not shown). To further confirm the existence of a direct interaction between Arp3 and the N-terminus of the CA peptide, the DOPA(462)-CA peptide was incubated at a final concentration of 20 nM with increasing concentrations of the Arp2/3 complex, cross-linked, and analyzed by Western blotting against biotin and several proteins within the complex (Figure 5b). In the presence of the DOPA(462)-CA peptide a biotinylated product was detected when incubated with 100 nM, 500 nM, and 1 μM Arp2/3 complex (top panel). As expected, the cross-linked product was recognized with α-Arp3 but not α-Arp2, α-ARPC1, or α-ARPC3, confirming that the DOPA(462)-CA peptide cross-links specifically with Arp3.

DISCUSSION

A straightforward way to dissect the interactions of the CA peptide with the Arp2/3 complex is to examine each functional segment of the peptide. Previous investigations have yielded conflicting results concerning the Arp2/3 complex subunit(s) that bind the A region of the VCA. One study found that deletion of the eight C-terminal amino acids

of N-WASP VCA abrogates cross-linking to Arp3, but not to Arp2 or ARPC1, suggesting that the binding site for the A region and its conserved Trp is located on Arp3 (14). These data are also consistent with homology modeling (17). In contrast, VCA peptides from WASP and the yeast WASP-like protein, Bee1, were found to bind to the isolated yeast ARPC1 subunit in a manner that depended on their C-terminal tryptophan side chains, suggesting that the A region also binds to ARPC1 in the intact assembly (16). In the crystal structure of the inactive Arp2/3 complex, ARPC3 and ARPC1 are ~ 50 Å apart. The SDSL data here indicating the spin label attached to Cys506 is within ~ 25 Å of ARPC3 are thus more consistent with a binding site on Arp3, which is immediately adjacent to ARPC3. However, a large conformational change upon Arp2/3 complex activation that would bring ARPC1 into closer proximity to ARPC3, as suggested by recent FRET analyses (5), could allow an ARPC1-bound 506* to induce line broadening in ARPC3 resonances.

The observed broadening of ARPC3 methyl signals caused by spin labels at positions 481 and 506 is of comparable magnitude, suggesting that these two positions are located at similar distances from the body of ARPC3. As above, the simplest interpretation of these data would also place residue 481, and the C-terminus of the C region, near the ARPC3/Arp3 interface, although other binding sites in a rearranged assembly cannot be excluded.

The NMR and cross-linking data also have implications about the relative position of the remainder of the C region. The spin label at position 462 has no effect on the intensities of methyl signals in ARPC3, suggesting that in the complex of Arp2/3 with CA peptide the N-terminus of the C region projects away from ARPC3. The cross-linking experiments presented here indicate CA interactions with Arp3, Arp2, ARPC1, and ARPC3. The cross-links to Arp2 and ARPC1 are particularly interesting. These two subunits contact each other, and in the inactive Arp2/3 structure their junction lies across the main cleft from ARPC3. The cross-links suggest that some segment of the CA peptide may span between ARPC3 and Arp2. In the context of the SDSL data alone, this cross-link likely involves the C region, which could facilitate closure of the cleft between the two Arp subunits. This is difficult to reconcile, however, with the DOPA-mediated cross-linking data, which indicate an interaction of the N-terminus of the CA peptide with Arp3. An important caveat is that our analyses here were performed in the absence of actin. The actin monomer is believed to bind to both the V and C regions of the VCA during Arp2/3 complex activation (10, 19, 33). Thus, in the absence of actin, the C region may be mobile and able to make a variety of contacts, only some of which are functional during nucleation. Detection of the true functional contacts of the C region may require actin. In the future, cross-linking and/or NMR analyses in the presence of actin will address this issue.

In this context, we favor placement of the C region away from ARPC3 and proximal to Arp2/ARPC1 interface, which is consistent with the probable position of the V region-bound actin monomer required for filament initiation. This first monomer would likely make pseudo-short-pitch contacts to Arp2 and pseudo-long-pitch contacts to Arp3, creating a trimeric nucleus. Our proposed location of the C region would then orient the V region (and probably part of the C

region itself) appropriately to contact the incoming first monomer during filament nucleation.

The NMR data presented here do not provide residue-specific information about the interaction of spin labels on CA with ARPC3, as its resolution is limited by our present inability to assign methyl group chemical shifts of ARPC3 in the intact complex, as well as broad spin-label effects due to the length of the maleimide–nitroxide tether. We have been able to assign many of the methyl chemical shifts in isolated ARPC3 (not shown), and it was our initial hope that many assignments in the intact assembly could be directly mapped from those of the free protein. However, direct mapping is complicated by a combination of incomplete backbone and side chain assignments of free ARPC3, broad lines in both cases, methyl resonance overlap, and the significant chemical shift changes observed throughout the methyl spectrum on incorporation of ARPC3 into the Arp2/3 complex. Alternate methods for assignment of the labeled component, including site-directed mutagenesis and analysis of pseudo-contact shifts induced by paramagnetic agents incorporated at specific, known sites (34–36), will likely be necessary for resonance assignment in large, asymmetric systems such as the Arp2/3 complex. However, even in the absence of assignments, NMR data combined with complementary analyses can lead to mechanistic conclusions as we have demonstrated here.

The combined NMR and cross-linking data presented here suggest a bivalent interaction of CA with the Arp2/3 complex. The interaction is anchored at two points, with the extreme C-terminus and the C-terminus of the C region binding proximal to ARPC3. The model supports a mechanism of VCA-mediated activation of the Arp2/3 complex through stabilization of the activated structure by interactions with Arp2, ARPC3, and Arp3. Moreover, it suggests that the C region may contribute to closure of the cleft between Arp3 and Arp2, perhaps through contacts to ARPC1 and Arp2. It is likely, however, that biasing of the conformational equilibrium of the Arp2/3 complex toward the closed state by an isolated CA (or VCA) peptide is incomplete, based on cryo-EM data (37). Full activation is probably accomplished through combinatorial interactions of the VC element with the monomeric actin and/or interactions of the Arp2/3 complex with existing actin filaments (1, 38). The VCA-induced shift in the equilibrium may, however, be sufficient to allow generation of initial actin filaments, which then act cooperatively with the VCA to drive maximal activation of the Arp2/3 complex.

ACKNOWLEDGMENT

We thank Dr. Judit Loconzci and Margaret Roberts-Abbott for organizing spectrometer time at the Varian Instruments facility in Palo Alto, CA. We also thank Chris Beltzner, Tom Pollard, and Bruce Goode for graciously sharing data prior to publication.

SUPPORTING INFORMATION AVAILABLE

¹H/¹³C HSQC spectrum of the recombinant human Arp2/3 complex labeled at ARPC3. This material is available free of charge via the Internet at <http://pubs.acs.org>.

REFERENCES

1. Higgs, H. N., and Pollard, T. D. (2001) Regulation of actin filament network formation through ARP2/3 complex: activation by a diverse array of proteins, *Annu. Rev. Biochem.* 70, 649–676.

2. Robinson, R. C., Turbedsky, K., Kaiser, D. A., Marchand, J. B., Higgs, H. N., Choe, S., and Pollard, T. D. (2001) Crystal structure of arp2/3 complex, *Science* 294, 1679–1684.
3. Lorenz, M., Popp, D., and Holmes, K. C. (1993) Refinement of the F-actin model against X-ray fiber diffraction data by the use of a directed mutation algorithm, *J. Mol. Biol.* 234, 826–836.
4. Nolen, B. J., Littlefield, R. S., and Pollard, T. D. (2004) Crystal structures of actin-related protein 2/3 complex with bound ATP or ADP, *Proc. Natl. Acad. Sci. U.S.A.* 101, 15627–15632.
5. Goley, E. D., Rodenbusch, S. E., Martin, A. C., and Welch, M. D. (2004) Critical conformational changes in the Arp2/3 complex are induced by nucleotide and nucleation promoting factor, *Mol. Cell* 16, 269–279.
6. Rodal, A. A., Sokolova, O., Robins, D. B., Daugherty, K. M., Hippenmeyer, S., Riezman, H., Grigorieff, N., and Goode, B. L. (2005) Conformational changes in the Arp2/3 complex leading to actin nucleation, *Nat. Struct. Mol. Biol.* 12, 26–31.
7. Martin, A. C., Xu, X. P., Rouiller, I., Kaksonen, M., Sun, Y., Belmont, L., Volkmann, N., Hanein, D., Welch, M., and Drubin, D. G. (2005) Effects of Arp2 and Arp3 nucleotide-binding pocket mutations on Arp2/3 complex function, *J. Cell Biol.* 168, 315–328.
8. Dayel, M. J., and Mullins, R. D. (2004) Activation of Arp2/3 complex: addition of the first subunit of the new filament by a WASP protein triggers rapid ATP hydrolysis on Arp2, *PLoS Biol.*
9. Panchal, S. C., Kaiser, D. A., Torres, E., Pollard, T. D., and Rosen, M. K. (2003) A conserved amphipathic helix in WASP/Scar proteins is essential for activation of Arp2/3 complex, *Nat. Struct. Mol. Biol.* 10, 591–598.
10. Marchand, J. B., Kaiser, D. A., Pollard, T. D., and Higgs, H. N. (2001) Interaction of WASP/Scar proteins with actin and vertebrate Arp2/3 complex, *Nat. Cell Biol.* 3, 76–82.
11. Machesky, L. M., and Insall, R. H. (1998) Scar1 and the related Wiskott-Aldrich syndrome protein, WASP, regulate the actin cytoskeleton through the Arp2/3 complex, *Curr. Biol.* 8, 1347–1356.
12. Zalevsky, J., Grigorova, I., and Mullins, R. D. (2001) Activation of the Arp2/3 complex by the *Listeria* acta protein. Acta binds two actin monomers and three subunits of the Arp2/3 complex, *J. Biol. Chem.* 276, 3468–3475.
13. Zalevsky, J., Lempert, L., Kranitz, H., and Mullins, R. D. (2001) Different WASP family proteins stimulate different Arp2/3 complex-dependent actin-nucleating activities, *Curr. Biol.* 11, 1903–1913.
14. Weaver, A. M., Heuser, J. E., Karginov, A. V., Lee, W. L., Parsons, J. T., and Cooper, J. A. (2002) Interaction of cortactin and N-WASP with Arp2/3 complex, *Curr. Biol.* 12, 1270–1278.
15. Hufner, K., Higgs, H. N., Pollard, T. D., Jacobi, C., Aepfelbacher, M., and Linder, S. (2001) The verprolin-like central (vc) region of Wiskott-Aldrich syndrome protein induces Arp2/3 complex-dependent actin nucleation, *J. Biol. Chem.* 276, 35761–35767.
16. Pan, F., Egile, C., Lipkin, T., and Li, R. (2004) ARPC1/Arc40 mediates the interaction of the actin-related protein 2 and 3 complex with Wiskott-Aldrich syndrome protein family activators, *J. Biol. Chem.* 279, 54629–54636.
17. Beltzner, C. C., and Pollard, T. D. (2004) Identification of functionally important residues of Arp2/3 complex by analysis of homology models from diverse species, *J. Mol. Biol.* 336, 551–565.
18. Kreishman-Deitrick, M., Egile, C., Hoyt, D. W., Ford, J. J., Li, R., and Rosen, M. K. (2003) NMR analysis of methyl groups at 100–500 kDa: model systems and Arp2/3 complex, *Biochemistry* 42, 8579–8586.
19. Higgs, H. N., Blanchoin, L., and Pollard, T. D. (1999) Influence of the C terminus of Wiskott-Aldrich syndrome protein (WASP) and the Arp2/3 complex on actin polymerization, *Biochemistry* 38, 15212–15222.
20. Torres, E., and Rosen, M. K. (2003) Contingent phosphorylation/dephosphorylation provides a mechanism of molecular memory in WASP, *Mol. Cell* 11, 1215–1227.
21. Gournier, H., Goley, E. D., Niederstrasser, H., Trinh, T., and Welch, M. D. (2001) Reconstitution of human Arp2/3 complex reveals critical roles of individual subunits in complex structure and activity, *Mol. Cell* 8, 1041–1052.
22. Delaglio, F., Grzesiek, S., Zhu, G., Vuister, G. W., Pfeifer, J., and Bax, A. (1995) NMRPipe: a multidimensional spectral processing system based on UNIX pipes, *J. Biomol. NMR* 6, 277–293.
23. Denison, C., and Kodadak, T. (2004) Toward a general chemical method for rapidly mapping multi-protein complexes, *J. Proteome Res.* (in press).
24. Hajduk, P. J., Augeri, D. J., Mack, J., Mendoza, R., Yang, J., Betz, S. F., and Fesik, S. W. (2000) NMR-based screening of proteins containing ¹³C-labeled methyl groups, *J. Am. Chem. Soc.* 122, 7898–7904.
25. Tugarinov, V., Sprangers, R., and Kay, L. E. (2004) Line narrowing in methyl-TROSY using zero-quantum ¹H-¹³C NMR spectroscopy, *J. Am. Chem. Soc.* 126, 4921–4925.
26. Battiste, J. L., and Wagner, G. (2000) Utilization of site-directed spin labeling and high-resolution heteronuclear nuclear magnetic resonance for global fold determination of large proteins with limited nuclear Overhauser effect data, *Biochemistry* 39, 5355–5365.
27. Fancy, D. A., and Kodadek, T. (1999) Chemistry for the analysis of protein–protein interactions: rapid and efficient cross-linking triggered by long wavelength light, *Proc. Natl. Acad. Sci. U.S.A.* 96, 6020–6024.
28. Fancy, D. A., Denison, C., Kim, K., Xie, Y., Holdeman, T., Amini, F., and Kodadek, T. (2000) Scope, limitations and mechanistic aspects of the photo-induced cross-linking of proteins by water-soluble metal complexes, *Chem. Biol.* 7, 697–708.
29. Higgs, H. N., and Pollard, T. D. (2000) Activation by Cdc42 and PIP(2) of Wiskott-Aldrich syndrome protein (WASP) stimulates actin nucleation by Arp2/3 complex, *J. Cell Biol.* 150, 1311–1320.
30. Rohatgi, R., Ho, H. Y., and Kirschner, M. W. (2000) Mechanism of N-WASP activation by CDC42 and phosphatidylinositol 4,5-bisphosphate, *J. Cell Biol.* 150, 1299–1310.
31. Archer, C. T., Burdine, L., and Kodadek, T. (2005) (submitted for publication).
32. Burdine, L., Gillette, T. G., Lin, H. J., and Kodadek, T. (2004) Peroxide-triggered cross-linking of DOPA-containing peptide–protein complexes, *J. Am. Chem. Soc.* 126, 11442–11443.
33. Miki, H., and Takenawa, T. (1998) Direct binding of the verprolin-homology domain in N-WASP to actin is essential for cytoskeletal reorganization, *Biochem. Biophys. Res. Commun.* 243, 73–78.
34. Gaponenko, V., Altieri, A. S., Li, J., and Byrd, R. A. (2002) Breaking symmetry in the structure determination of (large) symmetric protein dimers, *J. Biomol. NMR* 24, 143–148.
35. Gaponenko, V., Sarma, S. P., Altieri, A. S., Horita, D. A., Li, J., and Byrd, R. A. (2004) Improving the accuracy of NMR structures of large proteins using pseudocontact shifts as long-range restraints, *J. Biomol. NMR* 28, 205–212.
36. Pintacuda, G., Keniry, M. A., Huber, T., Park, A. Y., Dixon, N. E., and Otting, G. (2004) Fast structure-based assignment of ¹⁵N HSQC spectra of selectively ¹⁵N-labeled paramagnetic proteins, *J. Am. Chem. Soc.* 126, 2963–2970.
37. Volkmann, N., Amann, K. J., Stoilova-McPhie, S., Egile, C., Winter, D. C., Hazelwood, L., Heuser, J. E., Li, R., Pollard, T. D., and Hanein, D. (2001) Structure of Arp2/3 complex in its activated state and in actin filament branch junctions, *Science* 293, 2456–2459.
38. Kelly, A. E., Kranitz, H., Dotsch, V., and Mullins, R. D. (2004) in *The American Society for Cell Biology 44th Annual Meeting Abstracts*, The American Society for Cell Biology, Washington, DC.
39. Kraulis, P. J. (1991) MOLSCRIPT: A program to produce both detailed and schematic plots of protein structures, *J. Appl. Crystallogr.* 24, 946–950.

BI051065N